ELSEVIER

Journal of Nuclear Materials 299 (2001) 83–89

journal of nuclear materials

www.elsevier.com/locate/jnucmat

Effect of helium implantation on mechanical properties and microstructure evolution of reduced-activation 9Cr–2W martensitic steel

R. Kasada [a,*], T. Morimura [b], A. Hasegawa [c], A. Kimura [a]

[a] *Institute of Advanced Energy, Kyoto University, Gokasho, Uji, Kyoto 611-0011, Japan*
[b] *Institute for Materials Research, Tohoku University, Aoba-ku, Sendai 980, Japan*
[c] *Department of Quantum Energy, Tohoku University, Aoba-ku, Sendai 980, Japan*

Received 15 February 2000; accepted 4 July 2001

Abstract

A reduced-activation martensitic steel was implanted with helium up to 580 at. ppm by using 36 MeV α-beam between 353 and 423 K along with displacement damage up to 0.226 dpa. The implantation-induced increase in ductile–brittle transition temperature (DBTT) was estimated to be 98 K for the standard charpy V-notched (CVN) specimen implanted with 580 at. ppm He, through the conversion of small punch (SP) test results by an empirical relationship. It is clarified from comparison with neutron irradiation data that the increase in DBTT as well as implantation-induced hardening is interpreted simply in terms of displacement damage, suggesting that there is no significant effect of helium on both the irradiation hardening and the fracture toughness of the steel. No fracture mode change by the helium implantation was observed in the SP tests, showing a complete cleavage fracture mode in the lower shelf energy region. © 2001 Elsevier Science B.V. All rights reserved.

PACS: 61.82.Bg

1. Introduction

Fusion structural materials have been considered to be liable to suffer from embrittlement by transmutation helium as well as that by displacement damage caused by 14 MeV neutron irradiation [1]. It is well known that in austenitic stainless steels, which will be utilized for ITER, several tens of at. ppm of small amount of helium cause severe embrittlement accompanied by a change in the fracture mode from transgranular to intergranular cracking caused by bubble formation at grain boundaries [2]. Although reduced-activation martensitic steels (RAMS) have a superior resistance to irradiation-induced embrittlement and void swelling under fission neutron irradiation such as in FFTF/MOTA with low helium concentration [3–5], helium-induced embrittlement has been considered to be a critical issue of steel in fusion environment. Helium effects on ferritic steels have been investigated by various simulation techniques of fusion environment, such as isotope/spectra tailoring [6–9], dual-ion beam irradiation [10] and high-energy helium implantation [11–16]. Isotope tailoring methods using the two-step reaction of ^{58}Ni in the mixed-spectrum fission reactor such as HFIR showed a considerable increase in the ductile–brittle transition temperature (DBTT) for ferritic steels such as 9Cr–1MoVNb and 12Cr–1MoVW and the large DBTT shift was attributed to transmutation helium [6]. On the other hand, the authors reported that nickel-added RAMS showed remarkable irradiation hardening following irradiation at low temperature in Japan Material Test Reactor (JMTR) where the transmutation helium is estimated to be 10^{-2} at. ppm [17].

* Corresponding author. Tel.: +81-774 38 3478; fax: +81-774 38 3479.
E-mail address: kasada@iae.kyoto-u.ac.jp (R. Kasada).

PII: S0022-3115(01)00660-2

Helium implantation technique is one of the powerful methods to investigate the helium effect on mechanical properties using mini-sized specimen techniques, because it introduces enough content of helium into specimens without any doping elements. Previous helium implantation experiments of ferritic steels were usually limited to tensile tests and microstructural observation, and very limited work was carried out to investigate the effect on ductile–brittle transition behavior mainly because of the limitations of irradiation volume [12]. In the previous work [18], the authors investigated the effects of 120 at. ppm of helium on the DBTT of RAMS, and concluded that this amount of helium never enhanced the shift of DBTT and irradiation hardening. This was interpreted in terms of high trapping capacity of helium in the martensitic structure in RAMS.

The objective of this study is to investigate the effect of higher concentration of helium on ductile–brittle transition behavior of 9Cr–2W martensitic steel to evaluate the capacity for helium trapping.

2. Experimental

The chemical composition of the Japanese low-activation martensitic steel (JLM-1) used in this study is shown in Table 1. Heat treatments were given by normalizing for 30 min at 1323 K, air cooling and final tempering for 1 h at 1033 K followed by air cooling. The specimens were punched out as tens of 3 mm diameter disks with a thickness of 0.22 mm, which was smaller than the range (0.23 mm) of helium implantation.

All the specimens were irradiated with 36 MeV α-particles from the cyclotron accelerator in the Tohoku University (CYRIC) at a temperature between 353 and 423 K, which was measured with thermocouples fixed on the specimen holder and one of the specimens. The temperature measured for the latter was very unstable, but the specimen temperature during the implantation was estimated to be lower than 423 K because there was no feature indicating that the indium paste which was used for fixing specimens melted during the implantation. Helium was homogeneously implanted up to 120 and 580 at. ppm by using energy degrader wheels. The corresponding displacement damage doses were estimated to be 0.048 and 0.226 dpa, respectively, by the TRIM code calculation. The damage rate and the helium implantation rate were 8.7×10^{-7} dpa/s and 2.6×10^{3} at. ppm/dpa, respectively.

Small punch (SP) tests [18,19] were performed at a cross-head speed of 0.2 mm/min at temperatures from 77 to 293 K. Test temperature was measured with a thermocouple in contact with the lower die and controlled within an error of ± 1 K. Fig. 1 shows a schematic view of the SP test specimen holder and a typical example of the load–deflection curve with the definition of SP properties, such as SP-fracture energy and so on. The SP-DBTT was obtained by measuring the SP-fracture energy, which is defined as the total area below the SP load–deflection curve, at various test temperatures. The

Table 1
Chemical composition of the used steel, JLM-1

	C	Si	Mn	P	S	Cr	W	V	Ta	Ti	B
JLM-1 (wt%)	0.10	0.042	0.53	0.002	0.0014	9.03	2.06	2.06	0.051	0.021	0.0032

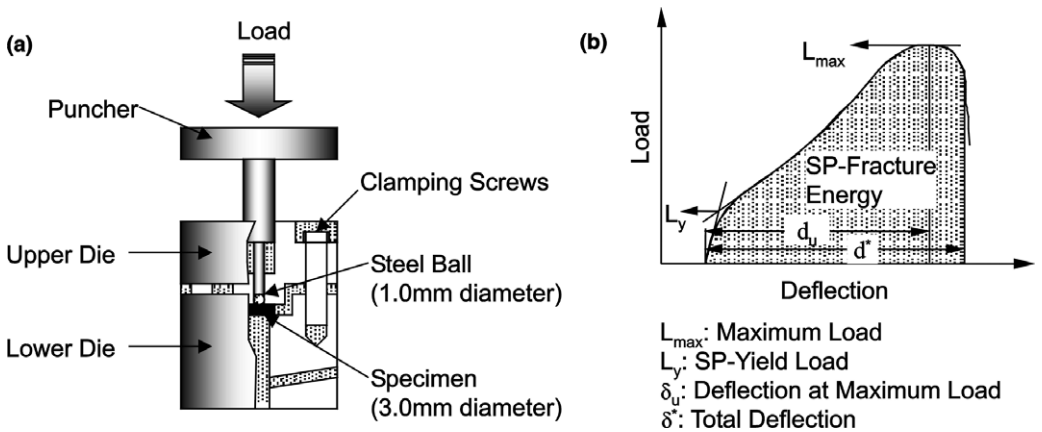

Fig. 1. Schematic view of (a) the specimen holder for SP test and (b) the definition of SP properties with a typical example of the load–deflection curve.

SP- DBTT is defined to be the temperature where the energy is the average of the maximum energy and the lower shelf energy. A disk of 3 mm diameter was grasped by dies along its peripheral edge and deformed by bulge deformation mode in a cold bath. Following SP tests, the surfaces of the fractured specimens were observed using scanning electron microscopy (SEM) to determine the fracture mode. Micro-Vickers hardness tests were performed with a load of 0.2 kg at room temperature after each implantation. Positron annihilation (PA) lifetime spectra were also measured at room temperature after each implantation, and then decomposed into two components, that is, a matrix component (τ_1, I_1) and a microvoid (V-cluster) component (τ_2, I_2), where τ_i and I_i were the lifetime and intensity of the ith component, respectively.

3. Results

3.1. SP properties and fracture behavior

Effects of helium implantation on the SP-DBTT curves are shown in Fig. 2, indicating that helium implantation-induced the shift of DBTT to higher temperature and the amount of shift appeared to increase with increasing helium concentration. The empirical relationship between the DBTT of SP test (SP-DBTT) and that of the standard CVN impact test (CVN-DBTT) has been obtained for many sorts of ferritic steels by the following equation [18]:

$$\text{CVN-DBTT}\ \ (\text{K}) = 2.5 \times \text{SP-DBTT}\ \ (\text{K}).$$

Increases in SP-DBTT (SP-ΔDBTT), which were 26 and 39 K for 120 and 580 at. ppm helium-implanted JLM-1, respectively, were thereby converted to CVN-ΔDBTT of 65 and 98 K, as summarized in Table 2.

Fracture surface observation following SP-tests revealed that the fracture mode of specimens implanted with helium up to 580 at. ppm was complete transgranular cleavage at temperatures below 112 K and intergranular cracking was never observed even in this region, while the fracture mode was ductile above 122 K, as shown in Fig. 3. There is a good correlation between fracture mode and SP-fracture energy.

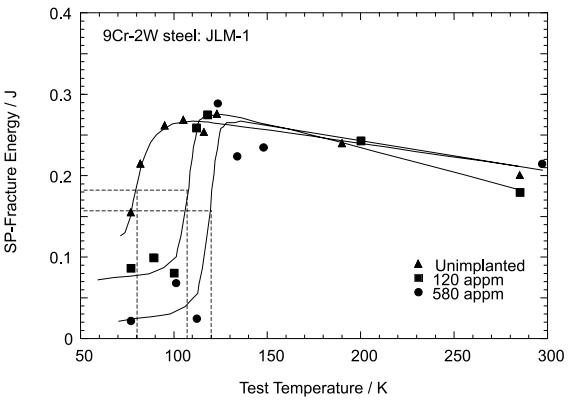

Fig. 2. Effect of helium implantation on the ductile–brittle transition curve of JLM-1 tested with SP-test.

3.2. Micro-Vickers hardness test

Helium implantation caused an irradiation hardening on the irradiation surface and also on the backside surface, as shown in Fig. 4. This suggests that the specimens were implanted with helium homogeneously through the specimen depth by utilizing the energy degrader. The increases in the hardness were 67 and 96 for specimens implanted with helium of 120 and 580 at. ppm, respectively, where the measured values were average increments in the implanted area. In order to compare the irradiation hardening due to helium implantation with that of neutron irradiation, the micro-Vickers hardness was converted into the tensile yield stress of which data are available for neutron-irradiated RAMSs. The empirical relationship between micro-Vickers hardness and tensile yield stress was derived from the experimental results of RAMSs irradiated in JMTR and expressed by the following equation [18]:

$$\sigma_y\ (\text{MPa}) = 1.54 \times H_\text{V} + 213\ \ (220 < H_\text{V} < 320).$$

The numerical data of micro-Vickers hardness measurements and the calculated yield stress are also shown in Table 2. The comparison to neutron irradiation will be discussed in the later section.

3.3. PA results

PA lifetime measurement is sensitive to detect small vacancy type defect clusters (V-cluster). The dose

Table 2
Numerical data of mechanical properties after helium implantation

	H_V	σ_y (MPa)	SP-DBTT (K)	CVN-DBTT (K)
Unimplanted	218	549	81	202
120 at. ppm	285	652	107	267
580 at. ppm	314	697	120	300

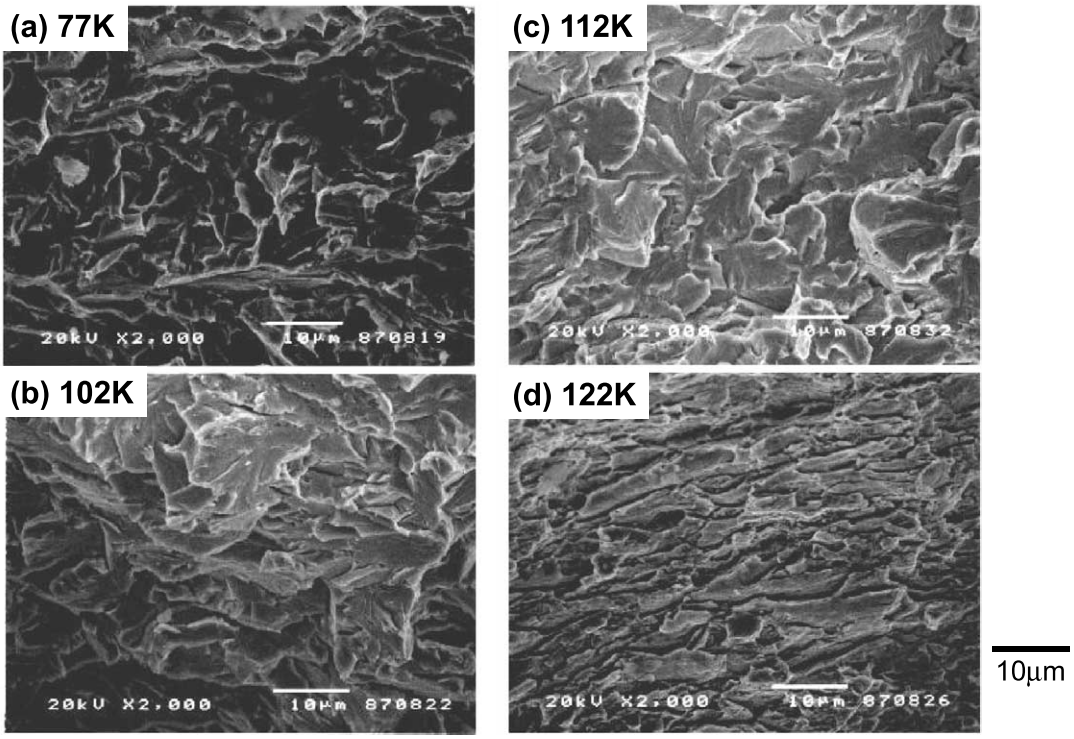

Fig. 3. Fracture surfaces of 580 at. ppm He-implanted specimens after SP tests at (a) 77 K, (b) 102 K, (c) 112 K and (d) 122 K. Specimens after SP tests above 122 K showed ductile failure.

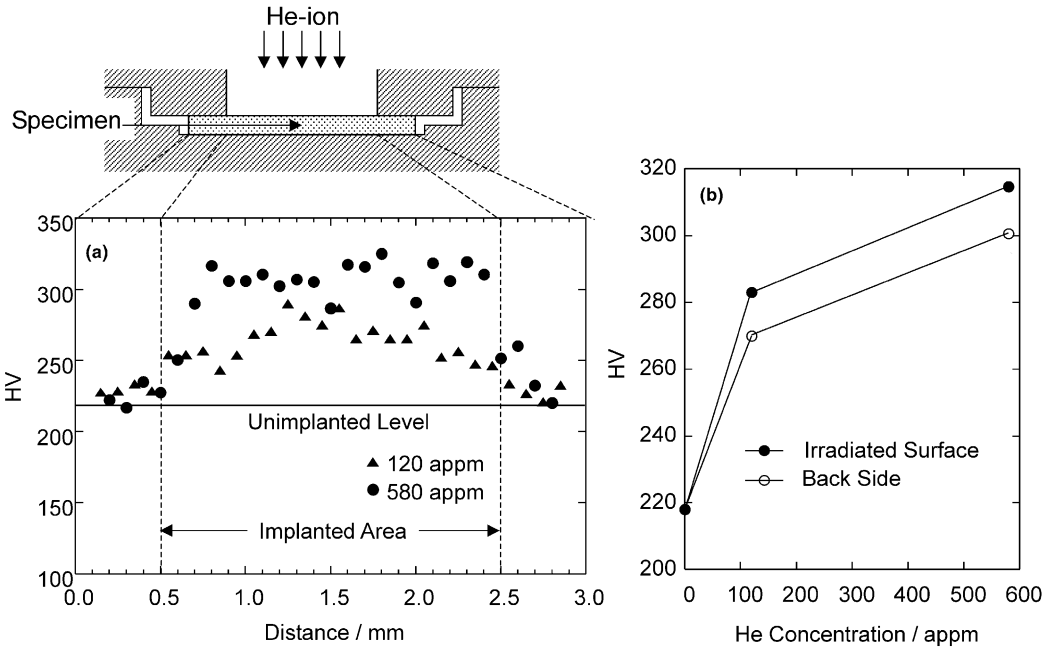

Fig. 4. (a) Vickers hardness distribution of implanted surfaces at 120 and 580 at. ppm helium implantation. (b) Dependence of Vickers hardness of the implanted surface and the back side on helium concentration.

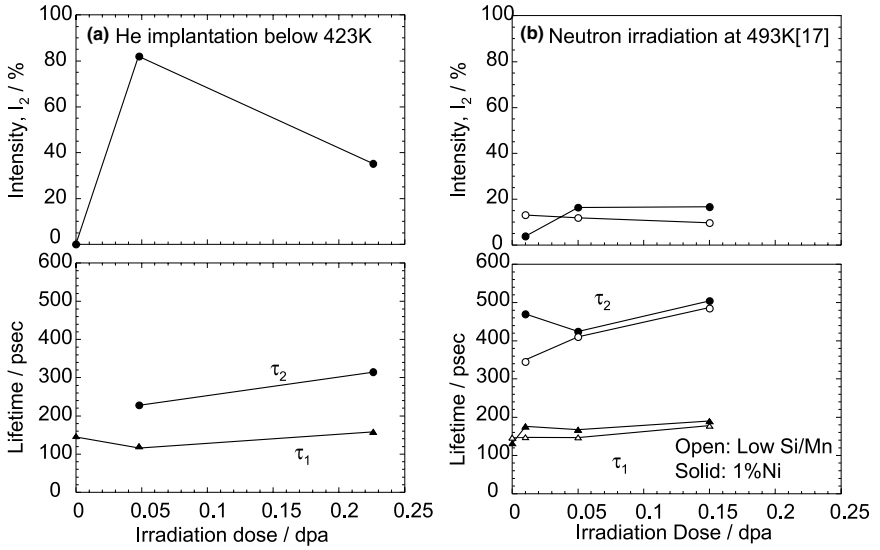

Fig. 5. Dose dependence of PA parameters in (a) helium-implanted JLM-1 and (b) neutron-irradiated 9Cr–2W steels in JMTR.

dependence of lifetime (τ_1, τ_2) and intensity of longer lifetime (I_2) of helium-implanted specimens are shown in Fig. 5(a) with those irradiated in JMTR at 493 K (Fig. 5(b)) [17]. The I_2 parameter of each helium-implanted specimen was much larger than that of the neutron-irradiated specimens, and τ_2 of the former was smaller than that of the latter, indicating that the V-cluster in helium-implanted specimens had higher density and smaller size than that of the neutron-irradiated one.

4. Discussion

4.1. Effects of helium on mechanical properties

4.1.1. Irradiation hardening

In order to investigate the effect of helium on irradiation hardening, the amount of hardening after helium implantation was compared with those of neutron-irradiated ferritic steels in JMTR, where the transmutation helium concentration was estimated to be 10^{-2} at. ppm at most for RAMS. As shown in Fig. 6, the dose dependence of the irradiation hardening of all the steels seems to follow the 1/4 power law as previously reported by the other researchers [20–22]. The slope of the linear relationship between σ_y and $(\mathrm{dpa})^{1/4}$ depends on the irradiation temperature and the slope becomes larger with decreasing irradiation temperature. The $\Delta\sigma_y s$ of helium-implanted steel, as plotted in the figure in comparison with neutron irradiation, were on a line between two lines of 353 and 493 K. Since the implantation temperature was between 353 and 423 K, the $\Delta\sigma_y s$ of helium-implanted steel are those which can be

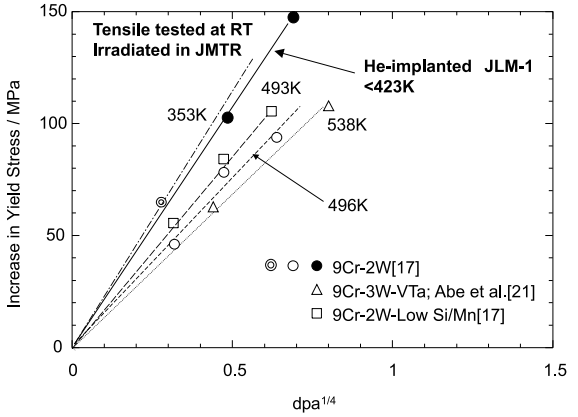

Fig. 6. Dose dependence of increase in the yield stress of 9Cr–2W steels, which follows 1/4 power of dpa.

expected from the dose and temperature dependence of neutron irradiation-induced hardening where transmutation helium is very small (10^{-2} at. ppm). Hence, irradiation hardening of helium-implanted JLM-1 is considered to be due to displacement damage and helium never causes enhancement of the hardening up to 580 at. ppm. It is expected that implanted-helium does not form helium clusters because of low mobility of helium below 423 K in the martensitic structure which contains a high density of trap sites for helium. Ullmaier and Camus [13] reported a similar result of the irradiation hardening behavior in the dual-beam or high-energy helium irradiated RAMS with the concentration up to 0.5 at.%; no enhancement of hardening was induced by helium.

4.1.2. DBTT shift

Previous investigations on irradiation embrittlement of light water reactor pressure vessel steels have shown linear dependence between ΔDBTT and $\Delta\sigma_y$ after neutron irradiation. As shown in Fig. 7, ferritic steels for fusion structural materials also show a linear relationship between them up to a dose of 40 dpa, although the irradiation conditions, such as temperature, dose and energy spectrum of neutrons, are different among experimental data [5]. The data obtained for helium-implanted steel are also plotted in the figure, indicating that the relationship is never influenced by the larger introduction of helium. Since the linear relationship between ΔDBTT and $\Delta\sigma_y$ is considered to be broken off if the fracture stress is changed by irradiation, no effect of helium implantation on the relationship suggests that helium does not cause any change in the fracture stress. This agrees with the results of fracture surface observation showing no change in the fracture mode by the helium implantation up to 580 at. ppm. Therefore, the same linear relationship of helium-implanted steel as neutron-irradiated ones reflects no effect of helium on both irradiation hardening and embrittlement.

It is of notice that the data of helium-implanted steel were obtained for very thin specimens, while the data of neutron-irradiated steels were obtained for bulk specimens. Good linear relationship of helium-implanted steel in Fig. 7, therefore, suggests that the mechanical properties, especially yield stress, of bulk specimen can be evaluated by small specimen technology such as SP-testing.

4.2. Helium trapping behavior

In this study, no cavity was observed in as helium-implanted JLM-1 by transmission electron microscopy (TEM) because the implantation temperature was so low that no cavity grew to visible size. In contrast, PA analysis could give us information about small V-clusters. Though it is difficult to estimate the density and size of V-clusters from PA results, we could roughly estimate the amount of helium trapped by V-clusters by means of positron trapping model.

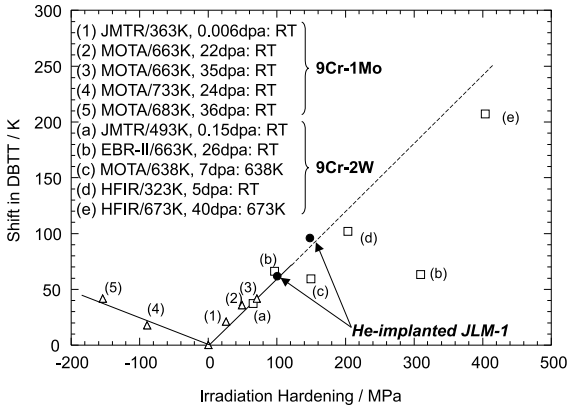

Fig. 7. Relation between irradiation hardening and shift in DBTT for neutron-irradiated 9Cr steels and helium-implanted JLM-1.

The density of microvoids C_V can be estimated as

$$C_V = \kappa/\mu. \tag{1}$$

The trapping rate κ is given by the formula

$$\kappa = [I_2/(1 - I_2)][(1/\tau_b) - (1/\tau_2)], \tag{2}$$

where τ_b is the positron lifetime in defect-free bulk, which is 110 ps in iron [23]; μ is the specific trapping rate for the V-cluster, and can be given by

$$\mu = N_V \mu_{1V}, \tag{3}$$

where N_V is the number of vacancies in a V-cluster, on which positron lifetime depends. Correlation between τ_2 and N_V was shown for iron by theoretical study [23]. μ_{1V} is the specific trapping rate for a vacancy, which was of the order of 10^{15} s^{-1} for all metals [24]. The total concentration of vacancies included in V-clusters can be obtained by $C_V N_V$. Thus, the He/V ratio, R, can be estimated by the following equation:

$$R = C_{He}/(N_V C_V) = C_{He}/(\kappa/\mu_{1V}). \tag{4}$$

The R-value of 580 at. ppm helium implantation is estimated to be 110 under the assumption that all the implanted-helium was trapped by microvoids, which is calculated directly from experimental data of I_2 and τ_2 when ignoring helium effect on lifetime. Since He/V ratio is considered to be not larger than 10, as expected by calculation study [25] and supported by SANS result [26], the above-mentioned R value of 110 appears to be over-estimated. To elucidate the reason for this disagreement, the trapping effect of helium on the positron lifetime in V-clusters was taken into account at first. It was reported that the lifetime of 500 ps for microvoid containing no helium in aluminum is reduced to about 200 ps in case that helium/vacancy (He/V) ratio is 2, because the lifetime of microvoid containing several helium atoms is shortened by the increase in the electron density [27]. However, in order to explain the over-estimation of R-value in terms of helium effect on lifetime, τ_2 would be changed by more than one order of magnitude, which is considered to be too large change when compared with the case of aluminum. Therefore, our result strongly suggests that the assumption that all the implanted-helium was trapped by microvoids is not realistic at all, and that there are another trapping sites for helium atoms, such as, dislocations, grain boundaries, lath-boundaries and carbides, in the martensitic structure of RAMS. According to the previous work on TEM

observation after helium implantation at higher temperature [11], nucleation of cavities was observed at dislocations and lath-boundaries as well as in the matrix. Thus, it is considered that a high resistance of RAMS to helium-embrittlement is due to high trapping capacity of the martensitic structure of the steel which prevents helium atoms from forming cavities and/or bubbles. Finally, it is concluded that the trapped helium atoms in martensitic structure never enhanced irradiation embrittlement up to the helium concentration of 580 at. ppm.

5. Conclusions

The ductile–brittle transition behavior and the microstructural evolution of reduced-activation martensitic steel (JLM-1 steel) after helium implantation up to 580 at. ppm at a temperature between 353 and 423 K were investigated. The main results are:

1. The SP-ΔDBTTs were 26 and 39 K for RAMS implanted with helium at 120 at. ppm (0.048 dpa) and 580 at. ppm (0.226 dpa), respectively. Converting the SP-ΔDBTT into ΔDBTT of standard Charpy test (CVN-ΔDBTT), corresponding CVN-DBTTs were estimated to be 65 and 98 K. The shift in DBTT is considered to be not due to helium but due to irradiation hardening caused by displacement damage.
2. No helium-induced enhancement of irradiation hardening was observed.
3. No intergranular cracking was observed in SP tested specimens even for those implanted with helium up to 580 at. ppm and broken in the lower shelf energy region.
4. PA measurements suggest that RAMS has many trapping sites for helium, such as dislocations and lath-boundaries, which is considered to be the main cause for high resistance to helium-induced embrittlement of RAMSs.

Acknowledgements

The authors are grateful to Professor K. Abe, graduate students in his laboratory, and CYRIC staff of Tohoku University for their help of helium implantation with a cyclotron. We would like to thank Professor M. Hasegawa for his advice on the PA lifetime measurement. We also thank the staff of Oarai branch, Institute for Materials Research, for utilizing hot laboratories.

References

[1] H. Ullmaier, Nucl. Fusion 24 (8) (1984) 1039.
[2] H. Schroeder, J. Nucl. Mater. 155–157 (1988) 1032.
[3] A. Hishinuma, A. Kohyama, R.L. Klueh, D.S. Gelles, W. Dietz, K. Ehrlich, J. Nucl. Mater. 258–263 (1998) 193.
[4] T. Morimura, A. Kimura, H. Matsui, J. Nucl. Mater. 239 (1996) 118.
[5] A. Kimura, M. Narui, T. Misawa, H. Matsui, A. Kohyama, J. Nucl. Mater. 258–263 (1998) 1340.
[6] R.L. Klueh, D.J. Alexander, J. Nucl. Mater. 218 (1995) 151.
[7] D.S. Gelles, G.L. Hankin, M.L. Hamilton, J. Nucl. Mater. 251 (1997) 188.
[8] P.J. Maziasz, R.L. Klueh, ASTM STP 1046 (1989) 35.
[9] K. Shiba, M. Suzuki, A. Hishinuma, J.E. Pawel, ASTM STP 1270 (1996) 753.
[10] N. Wanderka, E. Camus, H. Wollenberger, Mater. Res. Soc. Symp. Proc. 439 (1997) 451.
[11] A. Hasegawa, N. Yamamoto, H. Shiraishi, J. Nucl. Mater. 202 (1993) 266.
[12] R. Lindau, A. Möslang, D. Preininger, M. Rieth, H.D. Rohrig, J. Nucl. Mater. 271&272 (1999) 450.
[13] H. Ullmaier, E. Camus, J. Nucl. Mater. 251 (1997) 262.
[14] A. Hasegawa, H. Shiraishi, H. Matsui, K. Abe, J. Nucl. Mater. 212–215 (1994) 720.
[15] U. Stamm, H. Schroeder, J. Nucl. Mater. 155–157 (1988) 1059.
[16] A. Möslang, D. Preininger, J. Nucl. Mater. 155–157 (1988) 1059.
[17] R. Kasada, A. Kimura, H. Matsui, M. Narui, J. Nucl. Mater. 258–263 (1998) 1199.
[18] A. Kimura, T. Morimura, R. Kasada, H. Matsui, A. Hasegawa, ASTM STP 1366 (in press).
[19] T. Misawa, T. Adachi, M. Saito, Y. Hamaguchi, J. Nucl. Mater. 150 (1987) 194.
[20] W.C. Leslie, in: The Physical Metallurgy of Steels, McGraw-Hill Series in Mater. Sci. Eng., McGraw–Hill, New York, 1982, p. 269.
[21] F. Abe, M. Narui, H. Kayano, Mater. Trans., JIM 34 (11) (1993) 1053.
[22] P. Spätig, R. Schäublin, S. Gyger, M. Victoria, J. Nucl. Mater. 258–263 (1998) 1345.
[23] M.J. Puska, R.M. Nieminen, J. Phys. F 13 (1983) 333.
[24] R.M. Nieminen, J. Laakkonen, Appl. Phys. 20 (1979) 181.
[25] D.J. Reed, Radiat. Eff. 31 (1977) 129.
[26] G. Albertini, F. Carsughi, R. Coppola, W. Kesternich, G. Mercurio, F. Rustichelli, D. Schwahn, H. Ullmaier, J. Nucl. Mater. 191–194 (1992) 1327.
[27] K.O. Jensen, R.M. Nieminen, Phys. Rev. B 35 (4) (1987) 2087.